Images, Wavelets and PDE's, ICAOS'96, 285–294, Lecture Notes in Control and Inform. Sci., 219, Springer, 1996.

Biorthogonal Brushlet Bases for Directional Image Compression

François G. Meyer and Ronald R. Coifman

Department of Mathematics, Yale University, New Haven CT, 06520, USA.

Abstract–We construct new biorthogonal bases that provide precise frequency localization and good spatial localization. We develop a compression algorithm that exploits the bases to obtain a representation of the image in terms of textured patterns with different orientations, frequencies, sizes, and positions. The technique directly works in the Fourier domain and has potential applications for highly textured images.

1 Introduction

Edges and textures in an image can exist at all possible locations, orientations, and scales. The ability to efficiently analyze and describe textured patterns is thus of fundamental importance for image analysis and image compression. Edges can be characterized using a wavelet transform [1]. However, wavelets provide only an octave based decomposition of the Fourier plane with a poor angular resolution. Wavelet packets make it possible to adaptively construct an optimal tilling of the Fourier plane, and they have been used for image compression [2]. However a wavelet is always associated with two peaks in frequency that does not allow to selectively localize a unique frequency. We propose to segment the Fourier plane to obtain a precise representation of the image in terms of oriented textures with all possible directions, frequencies, and locations. To achieve this we have constructed new biorthogonal bases that we call *brushlets*. Each brushlet is accurately localized in the Fourier plane and is well localized in the position plane as well. The method consists in expanding the Fourier transform of a function into bases of smooth localized exponentials.

The paper is organized as follows. In the next section we review the construction of smooth localized orthonormal exponential bases. In section 3, we construct biorthogonal localized exponential bases. The new biorthogonal brushlet bases are described in section 4. The image compression algorithm that exploits a brushlet expansion, with results of experiments are given in section 5.

2 Local trigonometric bases

First we review the construction of smooth localized orthonormal exponential basis [3, 4]. These functions are exponentials with good localization in both position and Fourier space. We consider a cover $\mathbb{R} = \bigcup_{n=-\infty}^{n=+\infty} [a_n, a_{n+1}[$. We write

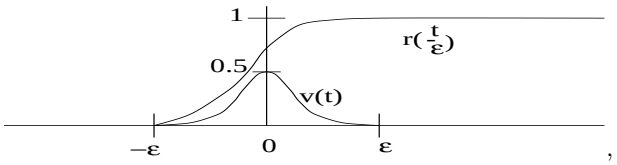

Fig. 1. Ramp function r, and bump function v.

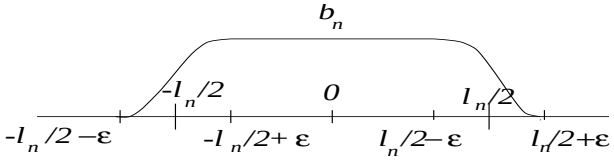

Fig. 2. Windowing function b_n.

$l_n = a_{n+1} - a_n$, and $c_n = (a_n + a_{n+1})/2$. Around each a_n we define a neighborhood of radius ε. Let r be a ramp function such that

$$r(t) = \begin{cases} 0 \text{ if } t \leq -\varepsilon \\ 1 \text{ if } t \geq \varepsilon \end{cases} \tag{1}$$

and

$$r^2(t) + r^2(-t) = 1, \qquad \forall t \in \mathbb{R} \tag{2}$$

Let v be the bump function supported on $[-\varepsilon, \varepsilon]$ (see Fig. 1)

$$v(t) = r(t)r(-t) \tag{3}$$

Let b_n be the windowing function supported on $[-l_n/2 - \varepsilon, l_n/2 + \varepsilon]$ (see Fig. 2)

$$\begin{aligned} b_n(t) &= r^2(t + l_n/2) \text{ if } t \in [-l_n/2 - \varepsilon, -l_n/2 + \varepsilon] \\ &= 1 \qquad\qquad\quad \text{if } t \in [-l_n/2 + \varepsilon, l_n/2 - \varepsilon] \\ &= r^2(l_n/2 - t) \text{ if } t \in [l_n/2 - \varepsilon, l_n/2 + \varepsilon] \end{aligned} \tag{4}$$

We consider the collection of exponential functions $e_{j,n} = e^{-2i\pi j(\frac{x-a_n}{l_n})}$, and we construct a basis of smooth localized orthonormal exponential functions $u_{j,n}$. Each $u_{j,n}$ is supported on $[a_n - \varepsilon, a_{n+1} + \varepsilon]$ and is given by [4]

$$u_{j,n}(x) = b_n(x - c_n)e_{j,n}(x) + v(x - a_n)e_{j,n}(2a_n - x) - v(x - a_{n+1})e_{j,n}(2a_{n+1} - x) \tag{5}$$

We have the following result [3, 4]

Theorem 1. [3, 4] *The collection* $\{u_{j,n}\ j, n \in \mathbb{Z}\}$ *is an orthonormal basis for* $L^2(\mathbb{R})$

We note that this basis uses exponentials, other smooth local bases that use sines, or cosines only can be also constructed [3, 5].

If we take the inverse Fourier transform $\check{u}_{j,n}$ of $u_{j,n}$ we obtain:

$$\check{u}_{j,n}(x) = e^{2i\pi c_n x}\left\{(-1)^j \widehat{b}_n(x - \frac{j}{l_n}) - 2i\, sin(\pi l_n x)\hat{v}(x + \frac{j}{l_n})\right\} \tag{6}$$

where $\widehat{b}_n$ is the Fourier transform of b_n, and $\hat{v}$ is the Fourier transform of v. The function $\check{u}_{j,n}$ is composed of two terms, localized around j/l, and around $-j/l$, that are oscillating with the frequency $c_n = (a_n + a_{n+1})/2$. In order to obtain a representation in terms of windowed exponentials we would like $\widehat{b}_n$ to be a positive windowing function. However, this constraint and the constraint (2) are incompatible. Therefore, we will relax condition (2), and construct two biorthogonal bases.

3 Biorthogonal Local trigonometric bases

We construct here biorthogonal bases of smooth localized exponentials. One basis can be used for the decomposition or analysis, and the other one for the reconstruction, or synthesis. We will proceed in a way similar to [6].

We consider here a cover $\mathbb{R} = \bigcup_{n=-\infty}^{n=+\infty}[a_n, a_{n+1}[$. All intervals have the same size $l = a_{n+1} - a_n$. Let $c_n = (a_n + a_{n+1})/2$. Let r be a ramp function such that

$$r^2(t) + r^2(-t) > 0, \qquad \forall t \in \mathbb{R} \tag{7}$$

Let v be the bump function supported on $[-l/2, l/2]$

$$v(t) = r(t)r(-t) \tag{8}$$

and let b be the windowing function supported on $[-l, l]$ (see Fig. 3).

$$\begin{array}{c} b(t) = r^2(t + l/2) \text{ if } t \in [-l, 0] \\ = r^2(l/2 - t) \text{ if } t \in [0, l] \end{array} \tag{9}$$

We choose r such that $\hat{b}$, the Fourier transform of b, is positive. An example of such b is the cubic spline:

$$C(x) = \chi_{[-1/2,1/2]} * \chi_{[-1/2,1/2]} * \chi_{[-1/2,1/2]} * \chi_{[-1/2,1/2]} \tag{10}$$

where $\chi_{[-1/2,1/2]}$ is the characteristic function of $[-\frac{1}{2}, \frac{1}{2}]$. C is compactly supported on $[-2, 2]$, as shown in Fig. 3. Since the Fourier transform of $\chi_{[-1/2,1/2]}$ is $\frac{\sin(\pi\xi)}{\pi\xi}$, the Fourier transform of C is

$$\hat{C}(\xi) = \left(\frac{\sin(\pi\xi)}{\pi\xi}\right)^4$$

The tail of $\hat{C}$ is rapidly decreasing to zero.

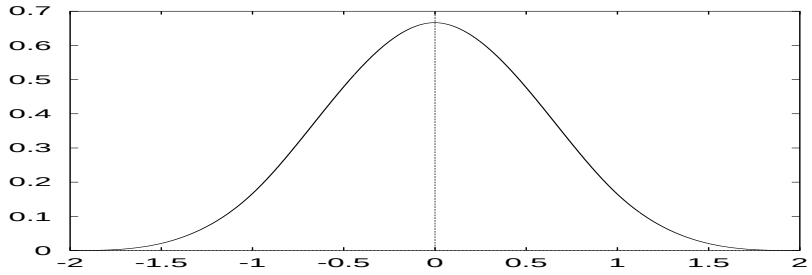

Fig. 3. Windowing function b, with $l = 2$

Let s be the l periodic function

$$s(x) = \frac{1}{\sum_{k\in\mathbb{Z}}\ r^2(x-a_k) + r^2(a_k - x)} \tag{11}$$

As above, we consider the collection of exponential functions

$$e_{j,n} = e^{-2i\pi j(\frac{x-a_n}{l})}$$

First we construct a basis of smooth localized orthonormal exponential functions $u_{j,n}$. Each $u_{j,n}$ is supported on $[a_n - l/2, a_{n+1} + l/2]$

$$u_{j,n}(x) = b(x-c_n)e_{j,n}(x) + v(x-a_n)e_{j,n}(2a_n - x) - v(x-a_{n+1})e_{j,n}(2a_{n+1} - x) \tag{12}$$

Then the dual basis is defined as

$$\tilde{u}_{j,n}(x) = s^2(x)u_{j,n}(x) \tag{13}$$

We have the following result

Lemma 1.

$$\int u_{j,n}(x)\tilde{u}_{k,m}(x)dx = \delta_{j,k}\delta_{n,m} \tag{14}$$

$\forall f \in L^2(\mathbb{R})$,

$$f(x) = \sum_{j,n} f_{j,n}u_{j,n}(x) \qquad \textit{with } f_{j,n} = \int f(x)\tilde{u}_{j,n}(x)dx \tag{15}$$

$$f(x) = \sum_{j,n} \tilde{f}_{j,n}\tilde{u}_{j,n}(x) \qquad \textit{with } \tilde{f}_{j,n} = \int f(x)u_{j,n}(x)dx \tag{16}$$

$u_{j,n}$ and $\tilde{u}_{j,n}$ are Riesz biorthogonal bases.

Proof. We first normalize the ramp function $r(t)$. Let

$$r^0(x) = \frac{r(x)}{\sqrt{r^2(x) + r^2(-x)}} \tag{17}$$

be the normalized ramp function that satisfies (2). We can then apply theorem 1 and construct a local exponential basis u^0

$$u^0_{j,n}(x) = b^0(x-c_n)e_{j,n}(x) + v^0(x-a_n)e_{j,n}(2a_n - x) \\ - v^0(x-a_{n+1})e_{j,n}(2a_{n+1}-x) \tag{18}$$

where $b^0(x)$ is the window function associated with r^0 defined by (4). Similarly, v^0 is the bump function associated with r^0 defined by (3).

If $x \in [a_n - l/2, a_n + l/2]$ then

$$u^0_{j,n}(x) = \frac{r^2(x-a_n)}{r^2(x-a_n)+r^2(a_n-x)}e_{j,n}(x) \\ + \frac{r(x-a_n)r(a_n-x)}{r^2(x-a_n)+r^2(a_n-x)}e_{j,n}(2a_n-x) \tag{19}$$

thus

$$u^0_{j,n}(x) = s(x)\left\{r^2(x-a_n)e_{j,n}(x) + r(x-a_n)r(a_n-x)e_{j,n}(2a_n-x)\right\} \tag{20}$$

and finally

$$u^0_{j,n}(x) = s(x)u_{j,n}(x) \tag{21}$$

Similarly, if $x \in [a_{n+1} - l/2, a_{n+1} + l/2]$ we get

$$u^0_{j,n}(x) = s(x)u_{j,n}(x) \tag{22}$$

We now use (21,22) and the fact that $u^0_{j,n}$ is an orthonormal basis to prove (14). We have

$$\int u_{j,n}(x)\tilde{u}_{j,n}(x)dx = \int s^2(x)u_{j,n}(x)u_{j,n}(x)dx \\ = \int u^0_{j,n}(x)u^0_{k,m}(x)dx = \delta_{j,k}\delta_{n,m}$$

Let $f \in L^2(\mathbb{R})$, in order to prove (15) we expand $f(x)s(x)$ into the basis $u^0_{j,n}$. We have

$$f(x)s(x) = \sum_{j,n}\{fs\}_{j,n}\ u^0_{j,n}(x) = \sum_{j,n}\{fs\}_{j,n}u_{j,n}(x)s(x) \tag{23}$$

with

$$\{fs\}_{j,n} = \int f(x)s(x)u^0_{j,n}(x)dx = \int f(x)s^2(x)u_{j,n}(x)dx = \int f(x)\tilde{u}_{j,n}(x)dx \tag{24}$$

thus from (23) and (24) we obtain

$$f(x) = \sum \int f(x)\tilde{u}_{j,n}(x)dx\ \ u_{j,n}(x). \tag{25}$$

In a similar way, if we expand f/s into the basis $u^0_{j,n}$ we obtain (16).

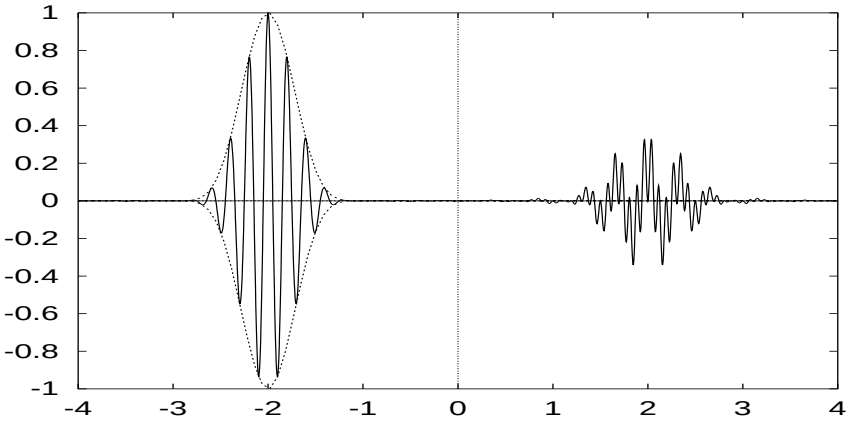

Fig. 4. Graph of the real part of $w_{j,n}$. On the left is the principal part of the brushlet: a windowed exponential. On the right is the part necessary to obtain perfect localization in Fourier space. In the two-dimensional case, with tensor products of brushlets, this part can be neglected.

4 Biorthogonal brushlet bases

4.1 One-dimensional case

We now construct the biorthogonal brushlet bases. We first construct two biorthogonal trigonometric bases $\{u_{j,n}, \tilde{u}_{k,m}\}$, with a ramp function $r(x)$ such that the Fourier transform of b is positive. Let $w_{j,n}$ be the Fourier transform of $u_{j,n}$ and let $\tilde{w}_{k,m}$ be the Fourier transform of $\tilde{u}_{k,m}$. Since the Fourier transform is a unitary operator, we have

Lemma 2. *$\{w_{j,n}, \tilde{w}_{k,m} j, k, m, n \in \mathbb{Z}\}$ are biorthogonal bases for $L^2(\mathbb{R})$*

We call $\{w_{j,n}, \tilde{w}_{j,n}\}$ the biorthogonal brushlet bases. We have

$$w_{j,n}(x) = e^{2i\pi c_n x} \left\{ (-1)^j \widehat{b}(x - \frac{j}{l}) - 2i \, sin(\pi l \, x) \hat{v}(x + \frac{j}{l}) \right\} \tag{26}$$

As explained above $w_{j,n}$ is composed of two terms, localized around j/l, and around $-j/l$, that are oscillating with the frequency $c_n = (a_n + a_{n+1})/2$. The first term is an exponential multiplied by the window $\widehat{b}_n$. The window of the second term is not positive. However the magnitude of the second term is smaller than the first one. Therefore we will consider that $w_{j,n}$ is mainly localized around $-j/l$. Figure 4 shows the graph of the real part of $w_{j,n}$ when we use the cubic spline for b.

4.2 Two-dimensional case

In the two-dimensional case we define two partitions of $\mathbb{R}$, $\bigcup_{n=-\infty}^{n=+\infty} [a_n, a_{n+1}[$, and $\bigcup_{m=-\infty}^{m=+\infty} [b_m, b_{m+1}[$. We write $l = a_{n+1} - a_n$, and $h = b_{m+1} - b_m$. We then

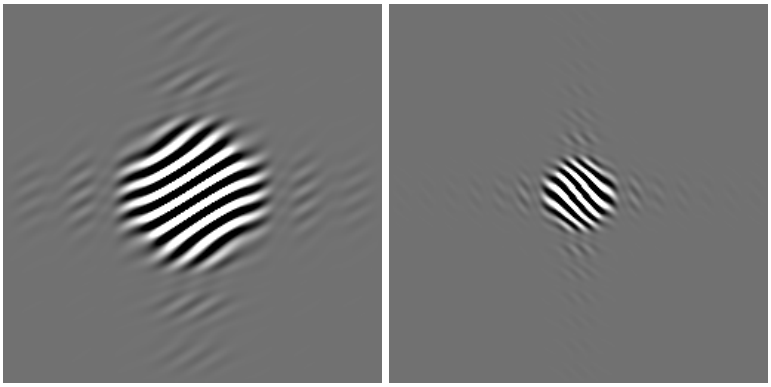

Fig. 5. Two dimensional brushlet basis functions $\{w_{j,n} \otimes w_{k,m}\}$ A good frequency resolution corresponds to a b with a small support, and is thus associated with a poor spatial resolution as shown on the left. A good spatial resolution corresponds to a $\hat{b}$ with a small support, and is thus associated with a poor frequency resolution as shown on the right.

consider the tilling obtained by the tensor products $[a_n, a_{n+1}[\otimes[b_m, b_{m+1}[$. We consider the separable tensor products of bases $w_{j,n}$, and $w_{k,m}$. We have

Lemma 3. *The sequences* $\{w_{j,n} \otimes w_{k,m}, \tilde{w}_{j',n'} \otimes \tilde{w}_{k',m'}\}$ *are Riesz biorthogonal bases for* $L^2(\mathbb{R}^2)$

The tensor product $w_{k,m}(x) \otimes w_{j,n}(y)$ is an oriented pattern oscillating with the frequency $((a_m + a_{m+1})/2, (b_n + b_{n+1})/2)$ and localized at $(k/h, j/l)$, as shown in Fig. 5. The size of the pattern is inversely proportional to the size of the analyzing window: $h \times l$ in the Fourier space. We note that the decomposition achieved by wavelet packets does not permit us to localize a unique frequency, for instance in the positive part of the Fourier space. Indeed two symmetric windows are always associated with a wavelet. As a result a wavelet packet expansion will require many more coefficients to describe a pattern with an arbitrary orientation; whereas the same pattern can be coded with a single brushlet coefficient.

5 Image compression

We have developed a compression algorithm that exploits the biorthogonal brushlet bases. We use $\tilde{w}_{j,n}$ for the decomposition and $w_{j,n}$ for the reconstruction. We use the cubic spline for b. We describe here a monoresolution of the algorithm, where all windows $[a_n, a_{n+1}[\otimes[b_m, b_{m+1}[$ have the same size. We are currently working on an adaptive multiresolution algorithm where the size of the window is selected according to the frequency content of the image.

5.1 Brushlet decomposition

The Fourier transform $\hat{f}$ of the image f is computed using a FFT. $\hat{f}$ is hermitian-symmetric, therefore we only retain the upper half of the Fourier plane $\{(\nu, \xi), \xi \geq 0\}$ for coding. We divide the upper half into two quadrants. For each quadrant we calculate the brushlet coefficients with square windows $[a_n, a_{n+1}[\otimes[b_m, b_{m+1}[$ of same size. Instead of calculating the inner product of $\hat{f}$ with $u_{j,n} \otimes u_{k,m}$ we fold the image around the horizontal and vertical lines associated with the tilling [4]. We then calculate the 2-D FFT of each folded block, and obtain the brushlet coefficients. Each block associated with this segmentation corresponds to a set of brushlet coefficients. These coefficients describe the intensity of one single "brush stroke" at different locations in the image, as illustrated in Fig. 5. This "brush stroke" has a particular frequency, orientation, and size, that are given by the position of the block, and its size.

5.2 Quantization and frequency scanning of the coefficients

The brushlet coefficients are quantized with uniform quantizers. In order to exploit the correlation between brushlet coefficients in different subbands, we order all the coefficients associated with the same spatial location by increasing frequency order. Since the magnitude of the terms in the sequence decreases with an exponential decay, we encode a terminating symbol after the last non-zero coefficient to indicate that the remaining coefficients are zeros. This represents a zero-tree like extension of the algorithm proposed in [7].

5.3 Entropy coding

After frequency ordering, the coefficients are entropy coded using variable length coding and an adaptive arithmetic coder. The first term of a frequency scan corresponds to a DC coefficient, and is therefore differentially encoded.

5.4 Experiments

We have implemented the coder and decoder, and an actual bit stream was created for each experiment. We present the results of the algorithm using two test images that are difficult to compress: 512x512 "Barbara", and 512x512 "Mandrill". The performance of the algorithm are summarized in Table 1, and results for compression ratios of 127:1 and 130:1 are shown in Fig. 3. We note that even at a compression ratio of 130:1 the mandrill still keeps its high frequency features such as the whiskers.

References

1. S. Mallat and S. Zhong. Characterization of signals from multiscale edges. *IEEE Trans. on Pattern Analysis and Machine Intelligence*, 14, 7:710–732, July 1992.

	Barbara
Compression	PSNR (dB)
7:1	31.03
14:1	26.98
31:1	24.15
56:1	22.65
63:1	22.31
74:1	21.95
86:1	21.54

Table 1. Coding results for 8bpp. 512x512 Barbara

	Mandrill
Compression	PSNR (dB)
5:1	28.68
10:1	24.64
28:1	21.84
45:1	21.1
63:1	20.71
76:1	20.52
95:1	20.35

Table 2. Coding results for 8bpp. 512x512 Mandrill

2. K. Ramchandran and M. Vetterli. Best wavelet packet bases in a rate-distortion sense. *IEEE Trans. on Image Processing*, 2(2):160–175, April 1993.
3. R.R. Coifman and Y. Meyer. Remarques sur l'analyse de Fourier à fenêtre. *C.R. Acad. Sci. Paris I*, pages 259–261, 1991.
4. M.V. Wickerhauser. *Adapted Wavelet Analysis from Theory to Software.* A.K. Peters, 1995.
5. I. Daubechies, S. Jaffard, and J.L. Journé. A simple wilson orthonormal basis with exponential decay. *SIAM J. Math. Anal.*, 22:554–572, 1991.
6. G. Matviyenko. Optimized local trigonometric bases. *Yale University, Department of Computer Science, Research report YALEDU/DCS/RR-1041*, 1994.
7. J.M. Shapiro. Embedded image coding using zerotrees of wavelet coefficients. *IEEE Trans. on Signal Processing*, 41(12):3445–3462, Dec. 1993.

Fig. 6. Barbara, compression 127:1

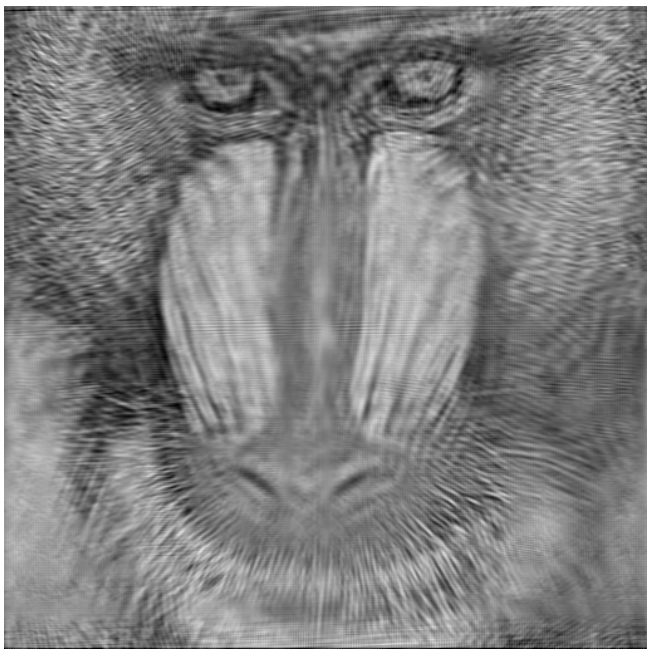

Fig. 7. Mandrill, compression 130:1.